

Experimental Study on Characteristics Variation of Permanent Magnets for High-speed Machine Applications*

Yunchong Wang^{1,2}, Hongxia Cao¹, Ilhami Colak³, Youhao Zhang¹ and Jianxin Shen^{1,2*}

(1. College of Electrical Engineering, Zhejiang University, Hangzhou 310027, China;

2. Zhejiang Provincial Key Laboratory of Electrical Machine Systems, Hangzhou 310027, China;

3. Department of Electrical and Electronics Engineering, Nisantasi University, Istanbul 34000, Turkey)

Abstract: High-speed permanent magnet (PM) electric machines are widely used. However, their extreme operating conditions, e.g., high temperature and high mechanical stress, lead to variations of the PM characteristics and affect the machine performance. In the present study, an experimental device is designed to test the PM characteristics by simulating the stress and temperature conditions of high-speed machines. The experimental results indicate that the PM remanence not only varies at high temperatures, which is well known, but also changes under high mechanical stress. It is shown that the PM remanence increases with the mechanical stress but decreases with the temperature rise. Accordingly, a new demagnetization-curve model of the magnets under multiple stresses is refined to better express the PM characteristics. The performance of a high-speed PM machine is then analyzed as an example to indicate the necessity of the model refinement. The effects of the temperature and mechanical stress on the conductivity of the PMs are also examined. The experimental results indicate that the conductivity of the PM increases with the temperature and pressure.

Keywords: High-speed machine, permanent magnet, mechanical stress, remanence variation, demagnetization-curve model

1 Introduction

Techniques of high-speed permanent magnet (PM) electric machines have been developed rapidly. Many applications, such as aeroengine spools, turbo compressors and centrifugal machines, utilize high-speed motor drives^[1-3]. However, high-speed PM machines still have many challenges in the aspects of design, manufacturing and application, such as loss distribution, stress distribution and heat dissipation^[4-5]. The maximum achievable power of high-speed PM machines is basically determined by the critical values of mechanical and thermal constraints, particularly the stress of the magnet^[6-8].

High-speed PM machines have the advantage of a high power density, i.e., a small size for a given power; thus, compared with regular-speed machines, their loss density is larger and the temperature rise of the rotor

can be higher. Moreover, the high temperature worsens the mechanical stress and magnetic properties of the magnets^[9].

Traditionally, when designing a high-speed PM machine, electromagnetic thermal iteration with the finite element method (FEM) is used to analyze the machine performance, in which the variations of PM characteristics with the temperature are taken into account^[10-11]. Excessive magnet temperatures pose a risk of irreversible demagnetization particularly when the motor is operated under field-weakening control^[12]. The effects of the temperature on the PMs and motor performance have been widely studied^[13-15].

However, in high-speed machines, the centrifugal force on the magnets is not negligible. To protect the magnets, a retaining sleeve is often employed, which applies a pre-compression on the magnets. Furthermore, when the rotor temperature rises, a thermal force is generated onto the magnets, since the magnets, retaining sleeve, and rotor yoke (or shaft) have different thermal expansion coefficients. Therefore, the magnets suffer from severe mechanical stresses, which may affect their characteristics. These

Manuscript received May 29, 2021; revised July 5, 2021; accepted August 11, 2021. Date of publication March 31, 2022; date of current version August 16, 2021.

* Corresponding Author, E-mail: J_X_Shen@zju.edu.cn

* Supported by the National Natural Science Foundation of China (51837010, 52007161), Zhejiang Provincial Natural Science Foundation (LQ20E070005), and Key R&D Program of Zhejiang Province (2019C01044).

Digital Object Identifier: 10.23919/CJEE.2022.000002

effects have hardly been studied.

In this study, an experimental device is designed and constructed to test the magnet characteristics under different temperature and mechanical-stress conditions. According to the test results, the demagnetization-curve model of the magnets is refined. As an example, a high-speed PM machine is analyzed using the original and refined models, respectively, in order to verify the necessity of the model refinement.

2 Operating conditions of PMs in high-speed motor

The parameters of the studied high-speed PM motor are presented in Tab. 1.

Tab. 1 High-speed PM machine parameters

Parameter	Value
Power/kW	250
Rated voltage/V	380
Rated speed/(r/min)	25 000
Number of stator slots	24
Number of poles	4
Stator outer diameter/mm	240
Stator inner diameter/mm	91
Rotor outer diameter/mm	86
Shaft diameter/mm	64
Stack axial length/mm	220

Four pieces of tile-shaped magnets are used in the machine. The temperature and mechanical-stress distributions in a piece of magnet under the rated torque and speed are shown in Fig. 1. The maximum temperature of the magnets is over 110 °C, and the compressive mechanical stress inside the magnets can reach approximately 46 MPa.

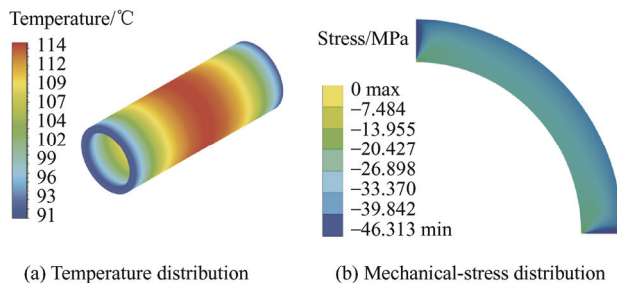


Fig. 1 Thermal and mechanical-stress analysis of the PM

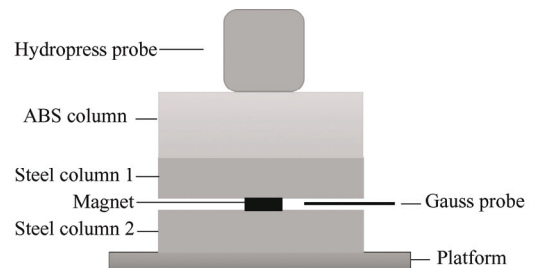
In this example, the electromagnetic thermal iteration has been applied, i.e., the magnet demagnetization-curve model in the final iteration is associated with the final temperature distribution.

However, the effects of the mechanical stress on the PM characteristics have not been considered. In the following sections, these effects will be studied.

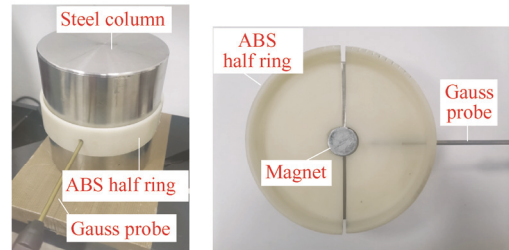
3 Influence of multiple stresses on PM remanence

3.1 Experimental device

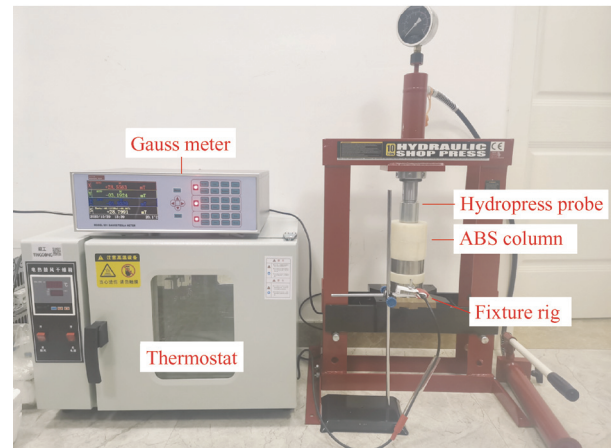
The designed experimental device is shown in Fig. 2a. The tested magnet column (or ring) with a small height is sandwiched between two steel columns. The magnet is heated with a thermostat in advance and protected with two acrylonitrile butadiene styrene (ABS) half rings before it is placed between the two steel columns, as shown in Figs. 2b and 2c. The ABS half rings are also for thermal isolation. They are slightly thinner than the magnet.



(a) Schematic



(b) Parts



(c) Whole test system

Fig. 2 Experimental device

A high-precision Gauss meter probe is placed inside the air gap between the steel columns with an individual fixture rig, to measure the air-gap field B_g . The position of the Gauss probe should not be changed during the test. A hydraulic presser is used to apply a pressure to the upper steel column and then the magnet. Because the hydropress probe and the frame of the presser are magnetic, there is flux leakage through the presser. Therefore, an ABS column is placed between the upper steel column and the hydropress probe, as shown in Fig. 2c, to isolate the magnetic circuit of the leakage flux.

It is assumed that the steel columns and the magnet do not deform when they are under pressure. However, the ABS column is softer and can deform. Therefore, it cannot be placed under the lower steel column; otherwise, the relative position of the Gauss probe inside the air gap will change when the pressure is applied. During the test, the magnet temperature decreased gradually and was measured using a non-magnetic thermometer. The thermometer is not shown in Fig. 2.

The steel columns (thickness of 50 mm, diameter of 100 mm) are far larger than the magnet (Tab. 2), and the air-gap length is identical to the magnet thickness. Therefore, the flux lines in the air gap are parallel. Additionally, they are perpendicular to the surfaces of the steel columns, as indicated by the FEM simulation results in Fig. 3.

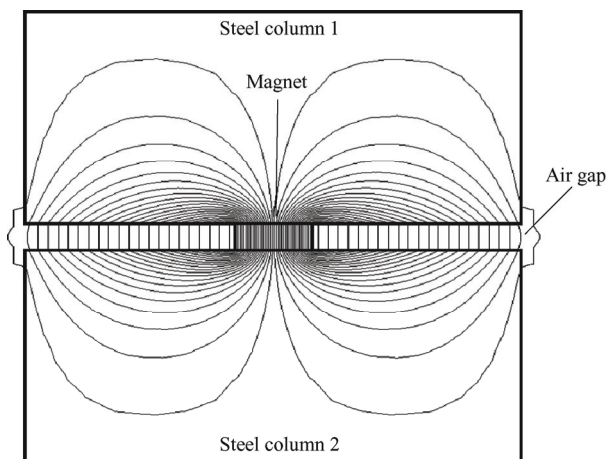


Fig. 3 Flux line distribution obtained with FEM

The B-H demagnetization-curve of the PM is linear. The original remanence B_r and coercivity H_c at room temperature and without extra mechanical stress are expressed with a subscript “0”, as shown in Fig. 4. It is assumed that the magnet permeability hardly changes

when the magnet is under multiple stresses (i.e., high temperature and mechanical stress within a workable range); thus, the demagnetization-curve shifts in parallel. The new B_r and H_c are expressed with a subscript “1”. Because the two steel columns have a large size, there is no magnetic saturation. Therefore, the load line of the magnet is linear, as shown in Fig. 4.

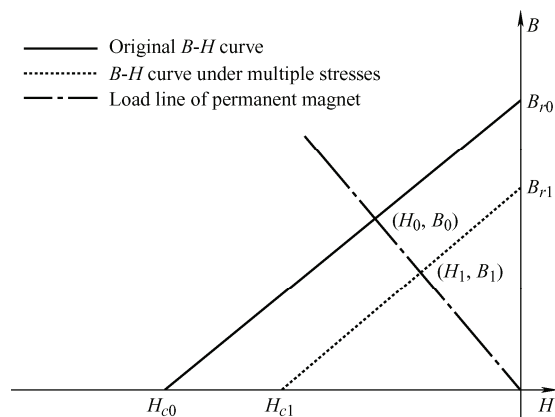


Fig. 4 Demagnetization curves and operating points of the PM

Clearly, the flux density B inside the magnet satisfies Eq. (1)

$$\frac{B_1}{B_0} = \frac{B_{r1}}{B_{r0}} \quad (1)$$

Moreover, the air-gap fields B_{g0} and B_{g1} , which are measured using the Gauss probe, are directly proportional to B_0 and B_1 . Therefore, from the measured B_g , the variation of the remanence B_r under multiple stresses can be derived, and the magnet demagnetization-curve model can be refined to better express the PM characteristics.

3.2 Test results and analysis

Six grades of commonly used sintered NdFeB magnets and two grades of sintered SmCo magnets were tested as examples. All the magnets were cylindrical. Their parameters are presented in Tab. 2.

Tab. 2 PM parameters

PM grade	Diameter/mm	Thickness/mm
NdFeB 38SH	31.5	6.5
NdFeB 40SH	18.0	6.5
NdFeB 42SH	22.0	6.5
NdFeB 45SH	18.0	6.5
NdFeB 38EH	15.0	6.5
NdFeB 40EH	35.0	6.5
SmCo GSM-30H	30.0	6.5
SmCo GSM-32H	30.0	6.5

3.2.1 Mechanical stress versus PM remanence

At room temperature of 25 °C, each grade of magnet was pressurized five times repeatedly, from 0 MPa to a maximum pressure value. The maximum pressure was that at which the magnet would start to crack; thus, it was not exactly the same among the magnet samples. The initial flux density of the PM remanence (B_{r0}) at 25 °C and under 0 pressure was set as a reference (i.e., 100%), and then the derived remanences at different pressures were plotted, as shown in Fig. 5.

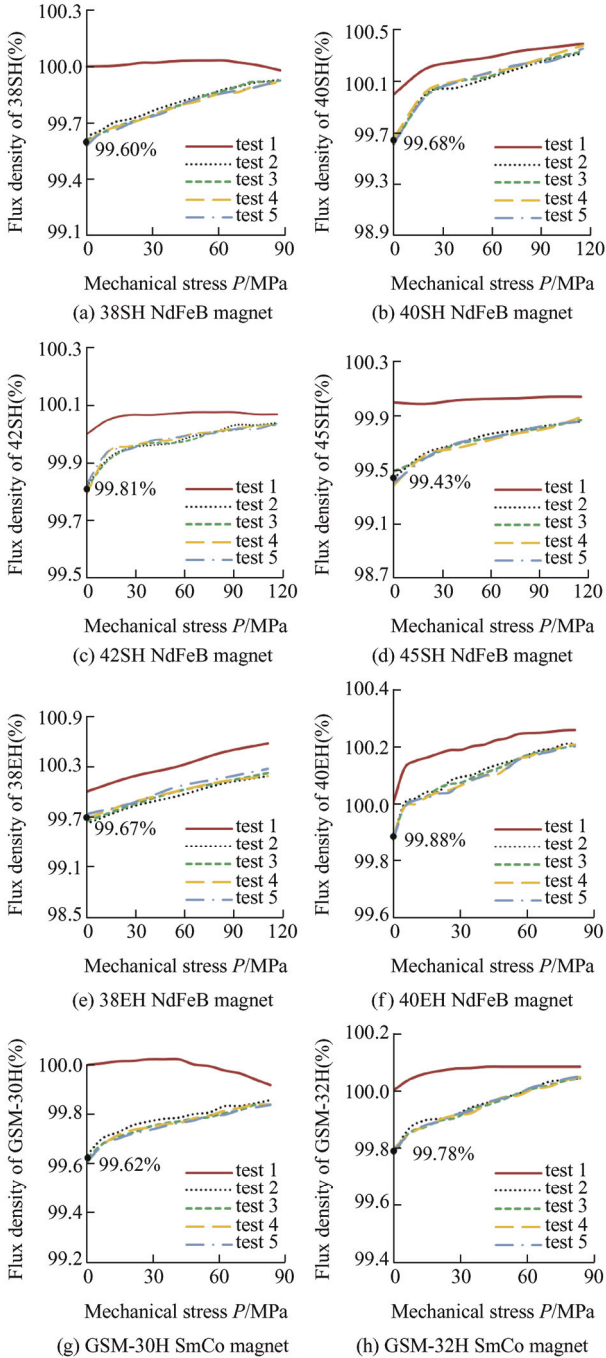


Fig. 5 Remanence variation of different PMs under different stresses at 25 °C

During the first pressurization process (see the curve of “test 1”), the PM remanence increased. However, when the pressure was released, the remanence did not return to 100% but decreased. For example, the remanence of the 38SH NdFeB magnet decreased to 99.60%, and that of the GSM-30H SmCo magnet decreased to 99.62%. Then, when the magnet was pressurized a second time, the remanence increased again (see the curve of “test 2”). For the third time or further pressurization, the variation of the PM remanence repeated, with little observable difference from the second time. The test results indicate that the magnet remanence was stabilized by the first pressurization.

In the test, three samples of each grade were measured, exhibiting almost identical values and variations of the remanence. Therefore, the test results are repeatable and reliable. Fig. 5 shows the average values for the three samples of each grade. The results for the 2nd-5th pressurizations were averaged for each magnet grade; thus, the stabilized remanence can be summarized as shown in Fig. 6.

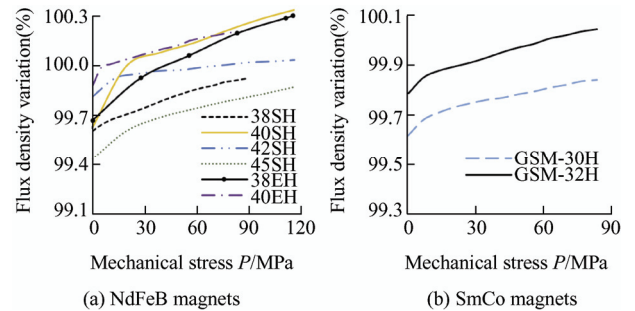


Fig. 6 Stabilized PM remanence under different stresses at 25 °C

For regular-speed PM machines, the initial remanence B_{r0} of the magnets can be used for the machine design. However, for high-speed machines, owing to the high stress in the magnets, which can reach tens or even hundreds of MPa, the stabilized remanence should be used.

3.2.2 Multiple stresses versus PM remanence

Besides the mechanical stress, the temperature rise places thermal stress on the magnets, whose effects on the PM characteristics have been reported. Therefore, the magnets were tested under different mechanical stresses and at different temperatures.

The results are shown in Fig. 7, where the stabilized remanence of the PM (i.e., the average result for tests 2-5) is presented. In each sub-figure of Fig. 7, there are 10 curves, which from the top to the bottom represent the data obtained at 25 °C, 30 °C, 40 °C, 50 °C, 60 °C, 70 °C, 80 °C, 90 °C, 100 °C and 110 °C, respectively.

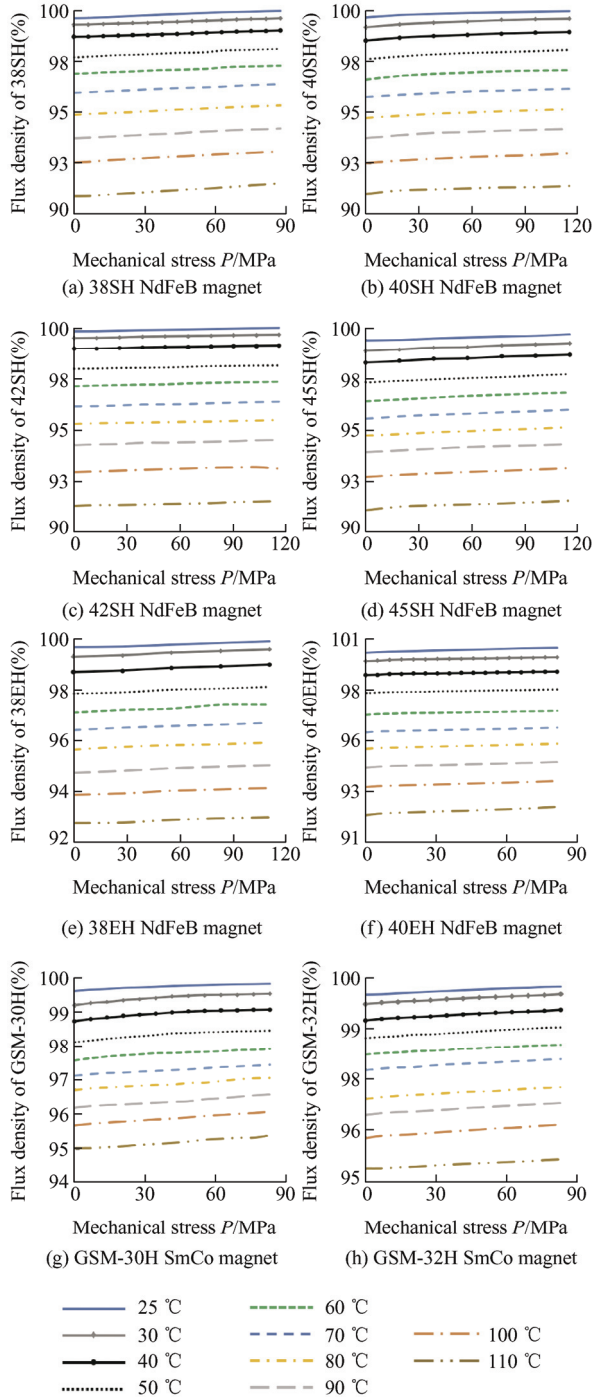


Fig. 7 Variation of PM remanence under different stresses at different temperatures

For each PM grade, the remanence increased slightly with the mechanical stress, which can be expressed by linear curve-fitting. Of course, the

variation of the GSM-30H PM can be better expressed with higher-order curve-fitting, as shown in Fig. 6b. However, from Fig. 7, it is known that the remanence variation under the mechanical stress is smaller than that under the temperature rise; therefore, linear curve-fitting is acceptable.

The remanence variation with the temperature rise is typically expressed via linear curve-fitting. The NdFeB materials had more significant variations than the SmCo materials. For example, when the magnet temperature increased from 25 °C to 110 °C, as shown in Fig. 1, the remanence of NdFeB decreased by approximately 9%, but that of the SmCo decreased by only approximately 4.5%.

According to the experimental results, the PM remanence B_r under the working conditions of temperature T and mechanical stress P can be expressed by Eq. (2), where the part with k_T represents the influence of thermal stress, the coefficient k_S reflects the PM property stabilization due to mechanical stress, and the part with k_P represents the influence of mechanical stress.

$$\begin{cases} B_r = f_{(T,P)} \cdot B_{r0} \\ f_{(T,P)} = [1 + k_T \cdot (T - 25)] \cdot k_S \cdot (1 + k_P \cdot P) \end{cases} \quad (2)$$

For the eight tested PM grades, the coefficients for Eq. (2) are presented in Tab. 3.

Tab. 3 Coefficients of curve-fitting for variation of PM remanence

PM grade	$k_T / (\times 10^{-4} \text{ } ^\circ\text{C})$	k_S	$k_P / (\times 10^{-5} \text{ MPa})$
NdFeB 38SH	-9.162	0.996 0	4.213
NdFeB 40SH	-9.169	0.996 8	3.202
NdFeB 42SH	-8.738	0.998 1	1.300
NdFeB 45SH	-9.543	0.994 3	6.098
NdFeB 38EH	-8.423	0.996 7	1.800
NdFeB 40EH	-8.190	0.998 8	3.100
SmCo GSM-30H	-4.432	0.996 2	4.920
SmCo GSM-32H	-4.478	0.997 8	2.300

Therefore, the magnet remanence under any working conditions can be determined, and then the linear demagnetization-curve model can be refined using this new remanence as well as the magnet permeability, which is assumed to be unaffected by the working conditions.

4 Performance analysis of high-speed machine with refined PM demagnetization-curve model

The motor electromagnetic performance, such as torque, current and losses, with different speeds and loads was calculated, and the corresponding temperature and mechanical-stress distributions at different positions of the magnets were computed using the FEM. When computing the mechanical stress, the interference fit between the magnets and the retaining sleeve, which causes significant extra mechanical stress, must be taken into account. Then, the magnets can be divided to pieces, assuming that each piece has an evenly distributed temperature T and mechanical stress P . Using the T and P , the demagnetization-curve model of each piece of the PM can be refined. Then, the motor electromagnetic performance is calculated again. Through such electromagnetic thermal iteration, the motor performance can be analyzed, with consideration of the variation of the PM characteristics under the temperature and stress. However, to simplify the computation, it is assumed that the magnets have an evenly distributed temperature and stress, for which the maximum T and P are taken, and one or two iterations are usually sufficient.

Here, the high-speed PM motor described in Section 2 is taken as an example, in which sintered 42SH NdFeB magnets are employed. The root-mean-square (RMS) value of the sine-wave armature currents is 555 A. Different temperatures (T) and mechanical stresses (P) of the magnets are considered.

The room temperature and steady-state operating temperature of the magnets are 25 °C and 110 °C, respectively. A P value of 0 MPa indicates that the mechanical-stress influence is ignored like the traditional analysis, whilst 100 MPa represents the influence of the total stress in the magnets. The RMS values of the terminal voltage (U) and the electromagnetic torque T_e with different T and P values are presented in Tab. 4, where the influence of the PM characteristics variation can be observed. The results confirm the necessity of the PM model refinement.

Tab. 4 Machine performance without/with refined PM model

Parameter	Without model refinement		With model refinement	
	$T=25$ °C, $P=0$ MPa	$T=110$ °C, $P=0$ MPa	$T=25$ °C, $P=100$ MPa	$T=110$ °C, $P=100$ MPa
U/V	372.1	344.5	372.6	345.1
$T_e/(N\cdot m)$	96.1	88.1	96.3	88.3

5 Influence of multiple stresses on PM conductivity

In high-speed PM machines, there is an eddy current in the PM. Clearly, the eddy current is related to the PM electric conductivity. Therefore, to investigate the effects of mechanical stress and thermal stress on the PM conductivity, a measurement device was designed for experimental study. A schematic of the device is shown in Fig. 8.

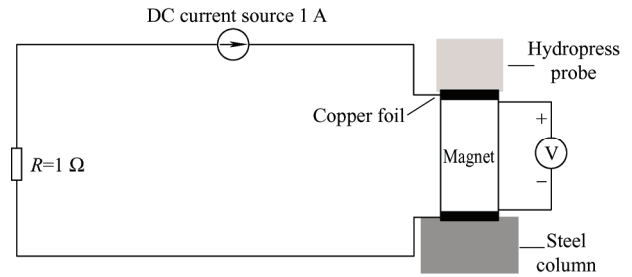


Fig. 8 Schematic of conductivity measurement

A high-precision direct current (DC) source was used, and its output in the test was set as 1 A. An external resistor of 1 Ω was connected in the circuit. Because the resistance of the tested PM was very low, the current source would be slightly unstable if this external resistor was not used. A high-precision digital DC voltage meter was used to measure the voltage drop on the PM.

The four-probe method was used to improve the measurement accuracy; thus, the column PM resistance could be determined, and the electric conductivity could be calculated using the PM diameter and length. To obtain smooth contact surfaces, copper foils were placed on the upper and lower surfaces of the column PM. During the experiment, mechanical stress was applied to the column PM with the hydropress probe, and the PM was heated to a certain temperature, simulating the working conditions in a high-speed PM machine.

The nominal conductivity of the tested PM was 625 000 S/m (from the datasheet). The PM was valid for the conditions of room temperature and zero compressive stress. The temperature coefficient of the conductivity is sometimes also provided in the datasheet.

Under different conditions of temperature and compressive stress, the actual electric conductivity changed, as shown in Tab. 5. The conductivity of the PM increased with increases in the mechanical stress and temperature. Clearly, such variations should be considered in multi-physics simulations of high-speed PM machines to enhance the simulation accuracy.

Tab. 5 Conductivity measurement results

Temperature/°C	Mechanical stress/MPa	Conductivity/ $[\times 10^5(\text{S/m})]$
20	0	6.103
	170	6.128
80	0	7.551
	170	7.756

6 Conclusions

It is well known that the characteristics of PMs, such as the remanence and electric conductivity, vary with changes in temperature. However, in high-speed machines, the magnets experience multiple stresses, such as high temperatures and strong mechanical compressive forces, and the effects of the multiple stresses (particularly the mechanical compressive stress) on the PM characteristics have not been reported.

In the present study, these effects were experimentally investigated using designed test devices. The PM remanence increased with the mechanical stress but decreased with the temperature rise. Moreover, after the first pressurization due to the mechanical stress, the PM remanence was slightly reduced but eventually stabilized. Therefore, the stabilized demagnetization-curve model of the magnets under multiple stresses was refined. The experimental results also indicated that the PM conductivity increased with increases in the mechanical stress and temperature. In high-speed PM machines, the magnets suffer from high temperatures as well as extreme mechanical stresses; therefore, the refined model is useful for improving the accuracy of

machine design and performance analysis.

References

- [1] J Shen, X Qin, Y Wang. High-speed permanent magnet electrical machines-applications, key issues and challenges. *CES Transactions on Electrical Machines and Systems*, 2018, 2(1): 23-33.
- [2] D Gerada, A Mebarki, N L Brown, et al. High-speed electrical machines: Technologies, trends, and developments. *IEEE Transactions on Industrial Electronics*, 2014, 61(6): 2946-2959.
- [3] D Miao, Y Mollet, J Gyselink, et al. Wide speed range permanent magnet synchronous generator design for a DC power system. *Chinese Journal of Electrical Engineering*, 2017, 3(1): 33-40.
- [4] G Jang, J Ahn, B Kim, et al. Design and characteristic analysis of a high-speed permanent magnet synchronous motor considering the mechanical structure for high-speed and high-head centrifugal pumps. *IEEE Transactions on Magnetics*, 2018, 54(11): 1-6.
- [5] G Du, W Xu, J Zhu, et al. Effects of design parameters on the multiphysics performance of high-speed permanent magnet machines. *IEEE Transactions on Industrial Electronics*, 2020, 67(5): 3472-3483.
- [6] A Tenconi, S Vaschetto, A Vigliani. Electrical machines for high-speed applications: Design considerations and tradeoffs. *IEEE Transactions on Industrial Electronics*, 2014, 61(6): 3022-3029.
- [7] Z Kolondzovski, A Arkkio, J Larjola, et al. Power limits of high-speed permanent-magnet electrical machines for compressor applications. *IEEE Transactions on Energy Conversion*, 2011, 26(1): 73-82.
- [8] Y Feng, F Li, S Huang, et al. Variable-flux outer-rotor permanent magnet synchronous motor for in-wheel direct-drive applications. *Chinese Journal of Electrical Engineering*, 2018, 4(1): 28-35.
- [9] C Zhang, L Chen, X Wang, et al. Loss calculation and thermal analysis for high-speed permanent magnet synchronous machines. *IEEE Access*, 2020, 8: 92627-92636.
- [10] G Du, W Xu, J Zhu, et al. Power loss and thermal analysis for high-power high-speed permanent magnet machines. *IEEE Transactions on Industrial Electronics*, 2020, 67(4): 2722-2733.
- [11] W Tong, R Sun, C Zhang, et al. Loss and thermal analysis of a high-speed surface-mounted PMSM with amorphous

metal stator core and titanium alloy rotor sleeve. *IEEE Transactions on Magnetics*, 2019, 55(6): 1-4.

- [12] T Huber, W Peters, J Böcker. A low-order thermal model for monitoring critical temperatures in permanent magnet synchronous machines. *7th IET International Conference on Power Electronics*, Manchester, UK, 2014: 1-6.
- [13] Y Wan, S Wu, S Cui. Choice of pole spacer materials for a high-speed PMSM based on the temperature rise and thermal stress. *IEEE Transactions on Applied Superconductivity*, 2016, 26(7): 1-5.
- [14] W Li, H Qiu, X Zhang, et al. Analyses on electromagnetic and temperature fields of superhigh-speed permanent-magnet generator with different sleeve materials. *IEEE Transactions on Industrial Electronics*, 2014, 61(6): 3056-3063.
- [15] Z Huang, J Fang, X Liu, et al. Loss calculation and thermal analysis of rotors supported by active magnetic bearings for high-speed permanent-magnet electrical machines. *IEEE Transactions on Industrial Electronics*, 2016, 63(4): 2027-2035.



Yunchong Wang was born in Liaoning, China, in 1987. He received the B.Eng. and M.Sc. degrees from Zhejiang University, Zhejiang, China, in 2010 and 2013, respectively, and Ph.D. degree from the Hong Kong Polytechnic University, Hong Kong, China, in 2017, all in Electrical Engineering. Since 2020, he has been an Associate Professor of Electrical

Engineering with Zhejiang University. He has authored more than 30 technical papers. His research interests include the design and control of permanent magnet machines, novel electrical motors for electrical vehicles, hybrid electrical vehicles and renewable energy conversion system.



Hongxia Cao received the B.S. degree from Zhejiang University, Hangzhou, China, in 2019. Currently, she is studying for her master's degree at Zhejiang University. Her current research interests include high-speed machine, permanent magnet and motor control.



İlhami Colak was born in 1962 in Turkey. He received his diploma in Electrical Engineering from Gazi University, Turkey in 1985. Then he did his MSc in Electrical Engineering in the field of Speed Control of Wound Rotor Induction Machines Using Semiconductor Devices at Gazi University in 1991. After that, he received his MPhil at Birmingham University in England in 1991. Finally, he got his PhD at Aston University

in England on Mixed Frequency Testing of Induction Machines Using Inverters in 1994. He became an Assistant Professor, an Associate Professor, and a Full Professor in 1995, 1999, and 2005, respectively. He has published more than 260 papers on different subjects. More than 144 of his papers have been cited in the SCI database of Thomson Reuters Web of Science (Clarivate Analytics). He is a member of IEEE, IES, IAS, PELS, and PES. In the last 10 years, he has concentrated his studies on renewable energy and smart grids. He is also the Editor-in-Chief of *International Engineering Technologies*, and one of the editors of *Journal of Power Electronics*. He also spent around 3 years at the European Commission Research Centre (JRC) as an expert in the field of smart grids in the Netherlands. He is currently holding the positions of Vice Rector and Dean of Engineering and Architecture Faculty of Istanbul Nisantasi University.



Youhao Zhang received the B.S degree form Harbin Institute of Technology, Harbin, China, in 2019. He is currently studying for his doctor's degree at Zhejiang University. His current research interests include soft magnetic materials applied for machine and iron loss calculation.



Jianxin Shen received the B.S. and M.S. degrees from Xi'an Jiaotong University, China, in 1991 and 1994. He received the Ph.D. degrees from Zhejiang University, China, in 1997. From 1997 to 1999, he studied as a Postdoctoral Fellow at Nanyang Technological University, Singapore. From 1999 to 2002, He was an Associate Researcher (meanwhile working towards a second Ph.D. degree, the degree awarded in July 2003) at Sheffield University, UK. From 2002 to 2004, he was a Research Engineer with IMRA Europe SAS, UK Research Centre, UK, a research centre associated with Aisin Seiki, Japan. Since 2004, he has been a Professor at Zhejiang University, China. He has published over 270 technical papers on journals or conferences, received 9 international paper awards and holds over 40 awarded patents. Prof. Shen has been a Senior Member of IEEE since 2002 and a Senior Member of CES since 2009. Since 2014, he has been a Fellow of IET.

His current research interests include electrical machine topologies, motor drives, motion control, applications, etc.